IOP Publishing Journal of Physics D: Applied Physics
J. Phys. D: Appl. Phys. **55** (2022) 025109 (8pp) https://doi.org/10.1088/1361-6463/ac2bc9

Impact of carbon–carbon defects at the SiO_2/4H-SiC (0001) interface: a first-principles calculation

Zhen Wang[1,4], Zhaofu Zhang[2,4], Sheng Liu[3], Chen Shao[1], John Robertson[2] and Yuzheng Guo[1,3,*]

[1] School of Electrical Engineering and Automation, Wuhan University, Wuhan 430072, People's Republic of China
[2] Department of Engineering, University of Cambridge, Cambridge CB2 1PZ, United Kingdom
[3] Institute of Technological Sciences, Wuhan University, Wuhan 430072, People's Republic of China

E-mail: yguo@whu.edu.cn

Received 30 June 2021, revised 13 September 2021
Accepted for publication 30 September 2021
Published 14 October 2021

Abstract

Poor quality of the SiO_2/4H-SiC (0001) interface is a long-standing issue limiting the performance of silicon carbide (SiC)-MOSFETs. However, the origin of the interface defects is still not fully understood. In this article, five types of carbon–carbon defects introduced to the SiO_2/4H-SiC (0001) interface are systematically investigated by first-principle calculations. The thermal oxidation process of 4H-SiC is analyzed through the variation of the chemical potentials based on the chemical reaction equation. The trend of the formation energy with different oxidation conditions show that oxygen-poor condition is effective to suppress the formation of carbon–carbon defects. We obtain the accurate electronic structure with hybrid density functional and the distribution of electron states for the carbon–carbon defects. The interfacial carbon–carbon defects in SiC tend to cause gap states near the conduction band minimum (CBM). Furthermore, the calculated charge transition levels (CTLs) also show that the 0/− CTLs of the carbon–carbon defects are close to the CBM acting as acceptors. All the theoretical calculation results provide insight into understanding the atomic structures and electronic properties for the carbon–carbon defects at the SiO_2/4H-SiC (0001) interface, which are fundamental to improve the performance of n-channel SiC-MOSFETs.

Supplementary material for this article is available online

Keywords: carbon–carbon defects, SiO_2/4H-SiC(0001) interface, gap states, conduction band minimum (CBM), n-channel SiC-MOSFETs

(Some figures may appear in color only in the online journal)

1. Introduction

Benefiting from the superior intrinsic physical properties, wide-band-gap (WBG) semiconductors have shown immense application potential for high-performance power devices [1, 2], among which silicon carbide (SiC) has been successfully commercialized. SiC has various polymorphs including 3C, 4H, 6H, etc [3]. 4H-SiC stands out with high bulk electron mobility (∼1200 cm^2 V^{-1} s^{-1} along (0001)) and WBG (3.26 eV), enabling 4H-SiC as the best candidate for power MOSFET manufacture [3, 4]. However, the practical performance of SiC-based MOSFETs is still far from its theoretical limits due to the poor interface with gate oxides [3].

[4] These authors contributed equally to this work.
[*] Author to whom any correspondence should be addressed.

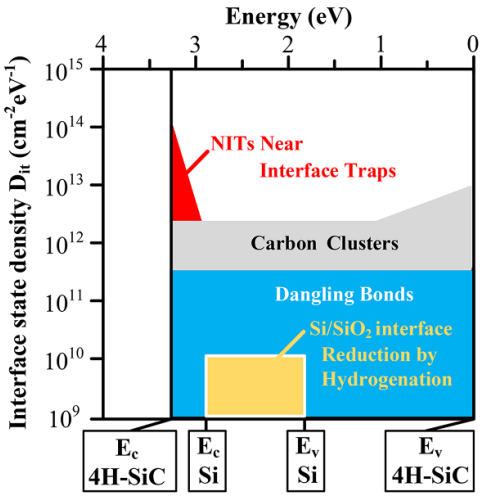

Figure 1. The composition of the interface state density (D_{it}) at the 4H-SiC/SiO_2 interface. E_V and E_C represent the valance band edge and conduction band edge, respectively. For comparison, the D_{it} of Si/SiO_2 interface is also shown. Reproduced with permission [5]. Copyright 2008, Wiley-VCH.

It is widely reported that a high interface state density (D_{it}) exists at the SiO_2/4H-SiC interface ($\sim10^{11}$–10^{14} eV^{-1} cm^{-2}), accounting for the low channel mobility and unstable operations [5–8]. Noborio *et al* conducted a series of experimental measurements on SiO_2/4H-SiC (0001) capacitors under different oxidation processes and reported that the D_{it} is mainly distributed near the conduction band edge (E_C) and valence band edge (E_V) of the SiC bandgap [9, 10]. The high D_{it} substantially originates from different types of defects at or near the SiO_2/4H-SiC interface (figure 1) [5, 11]. Different defect interface models are proposed by theoretical calculations or experiments to explain the defect origins, such as the sub-oxide layer [12, 13], the native point defects [14], the carbon-related defects including carbon-dangling bonds, SiC_xO_y species and carbon clusters [15–21]. Up to now, there is still no consensus for the unified model of the dominating defects. Although several passivation methods of post oxidation anneals (POAs) included H_2-POA, NO-POA, and $POCl_3$ are presented to improve the quality of the SiO_2/SiC interface (D_{it} decreased from $\sim10^{11}$ to $\sim10^{12}$ cm^{-2} eV^{-1}) [10, 12, 22–25], the channel mobility is still less than 10% of its bulk mobility [26]. Recently, Kimoto *et al* [27, 28] reported two approaches to obtaining a high-quality SiC (0001)/SiO_2 structures (D_{it} decreased to $\sim10^{10}$ cm^{-2} eV^{-1}), which one is depositing a thin silicon film on SiC, then followed by the low-temperature oxidation process of Si, the other is directly forming the SiO_2 film via chemical vapor deposition without SiC oxidation. However, for the traditional thermal oxidation process of SiC, further theoretical works are still needed.

Apart from the defect-trapped electrons, additional origins could also be responsible for the low electron mobility [29]. Referring to Si-based MOSFETs, carrier scattering also impacts the channel mobility, including surface roughness scattering, phonon scattering, and Coulomb scattering [30]. However, in the SiC-based device, the surface roughness scattering has a dominant impact on the field-effect mobility at a highly effective field (>1.5 MV cm^{-1}), while the actual mobility is still low under low effective field [30]. Phonon scattering has already been reported less impact on channel mobility [31]. Effects of Coulomb scattering can be restrained by reducing the D_{it}, but its practical impacts on increasing the channel mobility are still limited [32]. Ono has reported an additional scattering contributed by the internal-space states unique to the SiC [29]. However, considering the complexity of the thermal oxidation reaction of 4H-SiC, there may be accessional unsolved defects responsible for the high D_{it}, especially located at the conduction band edge limiting the channel mobility. From figure 1, D_{it} within the range of $\sim10^{11}$ and $\sim10^{12}$ cm^{-2} eV^{-1} is mainly related to the carbon-clusters.

In this work, we perform theoretical calculations to investigate five types of carbon–carbon defects at the SiO_2/4H-SiC (0001) interface, which are originated from the diffusion of carbon atoms during the oxidation process. First, we accurately reveal the atomic structures of carbon–carbon defects. To further understand the formation mechanism of defects, we calculate the variation of carbon and oxygen chemical potential based on the chemical reaction equation and analyzed the variation of the formation energy of two interfacial carbon–carbon defects under different oxidation conditions. Then we conduct the electronic structure analysis of the SiO_2/4H-SiC (0001) interface with carbon–carbon defects in detail and visually showed the distribution of defect states. We further calculated the charge transition levels (CTLs) of the defects. Finally, theoretical suggestions are given to improve the performance of n-channel SiC-MOSFETs based on the calculated results.

2. Methods

The interface supercell calculations were performed with the Vienna *ab initio* simulation package with projector-augmented-wave pseudopotential [33, 34]. A 5 × 3 × 1 Γ-centred Monkhorst–Pack [35] *k*-point grid with a cutoff energy of 500 eV was used for Brillouin zone sampling. The total energy was converged to be 10^{-6} eV/atom. The Perdew–Burke–Ernzerh of generalized gradient approximation exchange-correlation functional [36] was employed to optimize all the atomic geometries of the interfaces until the force of each atom converged below 0.02 eV $Å^{-1}$. All the electronic structures were calculated using Heyd–Scuseria–Ernzerhof hybrid functional (HSE06) [37] with Hartree–Fork fraction (α) of 0.23, which gives an accurate description of bandgap value ($\sim$3.20 eV) for 4H-SiC, consistent with the experimental value [30], but underestimates the band gap ($\sim$7.0 eV) of SiO_2. Here we focus on the distribution of the defect energy levels in the SiC bandgap, obtaining the accurate value of SiC bandgap is the priority, while the underestimation bandgap of SiO_2 has very little effect on our obtained results. The spin-polarization was considered for the charged defects calculation.

The SiO_2/4H-SiC interface created by matching ten atomic layers of α-quartz SiO_2 supercell with 12 layers of (0001) oriented bulk 4H-SiC supercell is used to investigate the

interfacial carbon–carbon defects. The interface models are built based on the dry oxidation interface model and the electron counting rule [38–40]. The detailed parameters of the basic model can be found in our previous work [40]. Although the actual thermal oxidation SiO_2 is amorphous, for the defect calculation, the local structure of the amorphous phase around the defect during the geometry optimization always has large deformation, which has an inevitable influence on the defect formation energy. However, the crystal interface model can suppress this demerit and give a relatively accurate energy comparison [20]. All the interface models include the 4H-SiC (0001) layers, the SiO_2 dielectric layers, different carbon–carbon defects, and a 20 Å thick vacuum layer.

3. Calculation results and analysis

3.1. Theoretical analysis of thermal oxidation and carbon–carbon defect models

SiO_2 dielectric layers are usually obtained by surface thermal oxidation of 4H-SiC. In the actual thermal oxidation process, the quality of the oxide layer depends on the oxidation conditions (wet or dry oxidation and temperature) as well as crystal surface orientation [9, 10, 41]. We mainly focus on its thermal dry oxidation process because 4H-SiC (0001) has the highest electron mobility. The ideal chemistry forming process of the SiO_2/SiC interface follows the reaction equation shown below:

$$\mathrm{SiC} + \frac{3}{2}\mathrm{O_2} \rightarrow \mathrm{SiO_2} + \mathrm{CO}.$$

However, the actual reaction process is complex and far from satisfactory. Critical factors that affected the reaction are the variation trends of carbon and oxygen chemical potential under different oxidation conditions [20]. We calculated the chemical potential variation values of Si, C and O under the chemical static equilibrium condition. The detailed chemical potentials calculation are followed as:

$$\begin{aligned}&\text{O-rich}: \ \mu_{\mathrm{O}} = \frac{1}{2}E(\mathrm{O_2}),\ \mu_{\mathrm{Si}} = E(\mathrm{SiO_2}) - 2\mu_{\mathrm{O}},\\ &\mu_{\text{C-rich}} = E(\mathrm{SiC}) - \mu_{\mathrm{Si}},\ \mu_{\text{C-poor}} = E(\mathrm{CO}) - \mu_{\mathrm{O}}, \qquad (1)\\ &\text{O-poor}: \mu_{\mathrm{O}} = \frac{1}{2}(E(\mathrm{SiO_2}) - \mu_{\mathrm{Si}}),\ \mu_{\mathrm{Si}} = E(\mathrm{Si}),\\ &\mu_{\text{C-rich}} = E(\mathrm{CO}) - \mu_{\mathrm{O}},\ \mu_{\text{C-poor}} = E(\mathrm{SiC}) - \mu_{\mathrm{Si}}, \qquad (2)\end{aligned}$$

where $E(\mathrm{Si})$, $E(\mathrm{SiC})$, $E(\mathrm{SiO_2})$, $E(\mathrm{O_2})$ represent the total energy of the unit cell for single-crystal Si, 4H-SiC, α-quartz SiO_2 and oxygen molecule (O_2), respectively. And μ_{O}, μ_{Si}, μ_{C} are the chemical potential of single O, Si and C atom, respectively. C-rich and C-poor conditions represent the upper bound and lower bound of the carbon chemical potential under corresponding oxidation condition, respectively.

μ_{C} has a large range of 8.95 eV and 5.72 eV in O-rich condition (-0.7 eV $< \mu_{\mathrm{C}} <$ 8.25 eV) and O-poor condition (-1.98 eV $< \mu_{\mathrm{C}} <$ 3.74 eV), respectively, while the variation range of μ_{C} in bulk SiC and CO are only 0.62 eV (formation enthalpy ΔH of 4H-SiC) and 1.10 eV (ΔH of CO), respectively. It is noted that all μ_{C} is referred to the single atom chemical potential of graphite (-10.55 eV). From our previous work [42], the interfacial Si component of SiC is preferentially oxidized, leading to lower interfacial μ_{O}. It indicates that although the interfacial C component can diffuse out of the interface by forming CO, considering the wide variation of μ_{C}, residual C atoms would trend to remain at the interface by producing carbon-related species under C-rich condition. Furthermore, we also give a detailed analysis from the thermochemical and oxidation kinetics viewpoints for the formation of carbon clusters [42].

Although many different kinds of defects have been reported, carbon-related defects have been experimentally and theoretically identified for causing high D_{it} [5, 8, 14–16, 18, 20, 42–44]. To evaluate the potential killers for the mobility of n-channel MOSFETs, five types of carbon–carbon (C = C) defect structures are specially considered, namely C_2–C = C–C_2, C_2–C = C–CO, Si_3–C–C–Si, and Si_2–C = C–Si_2, SiO–C = C–SiO, as shown in figure 2. They have been recognized as the potential defect structures related to the lower channel mobility [14–16, 20]. The 1st two models are formed by the residual C atoms diffusing into the interfacial Si vacancy. It is also recognized as a di-carbon anti-site defect [(C_2)Si] in SiC and identified as a stable defect [14, 20]. The average bond length between the two carbon atoms at the tetrahedral site is 1.39 Å and the Si–C length around the defects is 1.91 Å, close to the average length in the bulk (1.88 Å). This type of carbon–carbon defect structure does not lead to a significant change in the local tetrahedral structure. However, the C = C double bond is twisted to a dihedral angle of $\sim$90° rather than ideal 0°. The latter two types are established from the single C atoms diffusing into the C interstitial site of SiC and recognized as metastable [14]. The average bond length of C = C and adjacent Si–C are 1.38 Å and 1.80 Å, respectively. The 5th type is the interfacial di-carbon defect in SiO_2 side. All the detailed atomic structure parameters of defects are listed in table 1.

Besides, considering the actual growth of 4H-SiC channel is usually on 4°–6° off-axis Si-terminated 0001 substrate, it is unavoidable to form the stacking-fault defect at the interface [45, 46]. Here, we also introduce a stacking-fault type (stacking sequence is changed from ABCB to ACBA) [26] to the SiO_2/4H-SiC (0001) interface with carbon–carbon defects to further study its effect on the interface.

To examine the influence of the oxidization conditions on defects, we calculated variation of the formation energy of C_2–C = C–C_2 and C_2–C = C–CO defects under different conditions, as shown in figure 3. We can see that the formation energies of these two defects are quite low under O-rich and

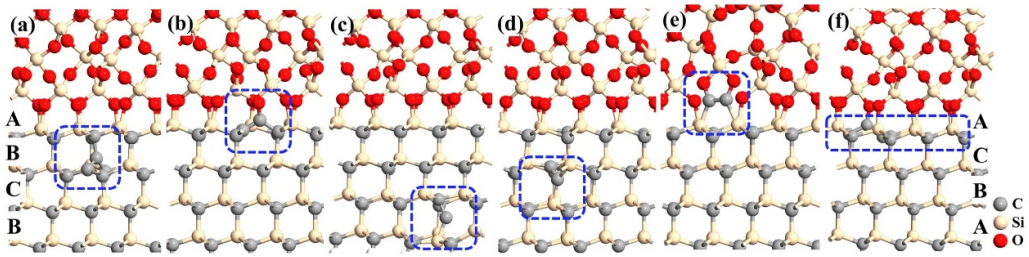

Figure 2. Fully relaxed structures of SiO_2/4H-SiC (0001) interface with (a) C_2–C = C–C_2, (b) C_2–C = C–CO, (c) Si_3–C = C–Si, (d) Si_2–C = C–Si_2, (e) SiO–C = C–SiO, and (f) stacking-fault carbon–carbon defect, respectively. Note that the normal stacking sequence of 4H-SiC atomic bilayers for the interface is ABCB, while the stacking-fault sequence is ACBA as labelled.

Table 1. Calculated bond length and angle parameters of the carbon–carbon defects. Note that all the values listed here are obtained from the fully relaxed structures.

	Bond length (Å)			Angle (°)		
Defect model	C = C	C–C	C–Si	∠Si–C–Si	∠C–C–C	Dihedral angle
C_2–C = C–C_2	1.42	1.52	1.98/1.90	—	136.97	88.06
C_2–C = C–CO	1.37	1.56	1.99/1.89	—	136.84	94.38
Si_3–C = C–Si	1.38	—	1.89/1.78	116.48	—	—
Si_2–C = C–Si_2	1.35	—	1.80/1.77	137.34	—	81.53
SiO–C = C–SiO	1.38	—	1.83/1.90	—	—	5.43

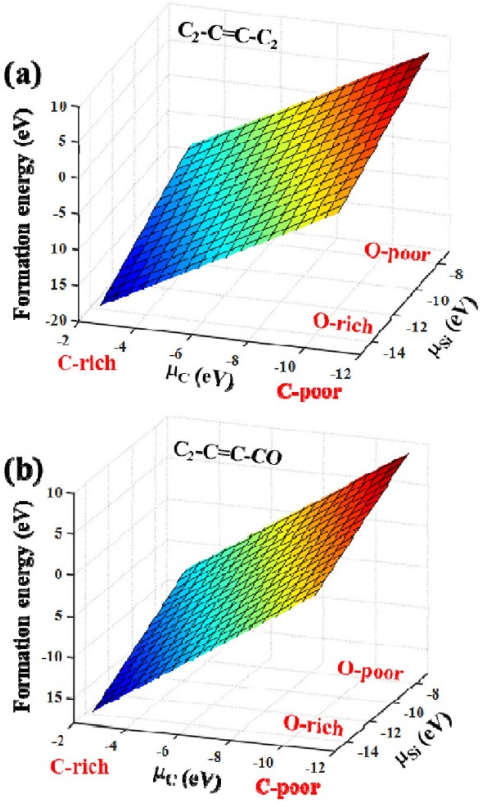

Figure 3. The variation trend of the defect formation energy versus the oxidation condition changes for (a) C_2–C = C–C_2, and (b) C_2–C = C–CO.

C-rich conditions. It indicates these two defects are more likely to be stable at the interface. As the oxidizing condition changes to O-poor, the formation energy of defects largely increase, which are hard to form. Therefore, considering the actual thermal oxidation process, O-poor condition is effective to suppress the formation of this type of carbon–carbon defect. But it does not mean that it can eliminate the defects. O-poor condition is a feasible measure to reduce the density of defects.

3.2. Electronic structure analysis

With the hybrid functional, the PDOS of the SiO_2/4H-SiC interfaces with C_2–C = C–C_2, C_2–C = C–CO, Si_3–C = C–Si, Si_2–C = C–Si_2, SiO–C = C–SiO, and defect-free cases in figure 4 are obtained from the slab models. From figure 4, gap states occur in the bandgap of all the defect interfaces and mainly localize at the di-carbon dimer where the defect sites. From the inserted orbitals (figure 4), gap states are mainly originated from the C–p anti-bonding orbitals. For C_2–C = C–C_2 defect, the peak of gap states lies at 1.16 eV below conduction band minimum (CBM). The gap states extend up to ∼0.3 eV below the CBM (figure 4(a)). For the C_2–C = C–CO defect, gap states mainly lie close to the mid-gap, but some gap states are also observed around the CBM (figure 4(b)). Apart from the C–p orbitals, the gap state is partially contributed by the interface O–p orbital. E_f here is lowered to 1.72 eV, due to the occupied O–p orbital. For Si_3–C = C–Si defect, two separated gap states exist. One lies at 0.52 eV below CBM and the other is located at 0.90 eV above the VBM (figure 4(c)), unfavorable for both n-channel and p-channel MOSFETs. For Si_2–C = C–Si_2 defect, the gap states mainly lie at the mid-gap, with some other delocalized gap states dispersed around the CBM (figure 4(d)). For the SiO–C = C–SiO defect, the gap states are very close to the VBM (∼0.6 eV below the VBM) (figure 4(e)).

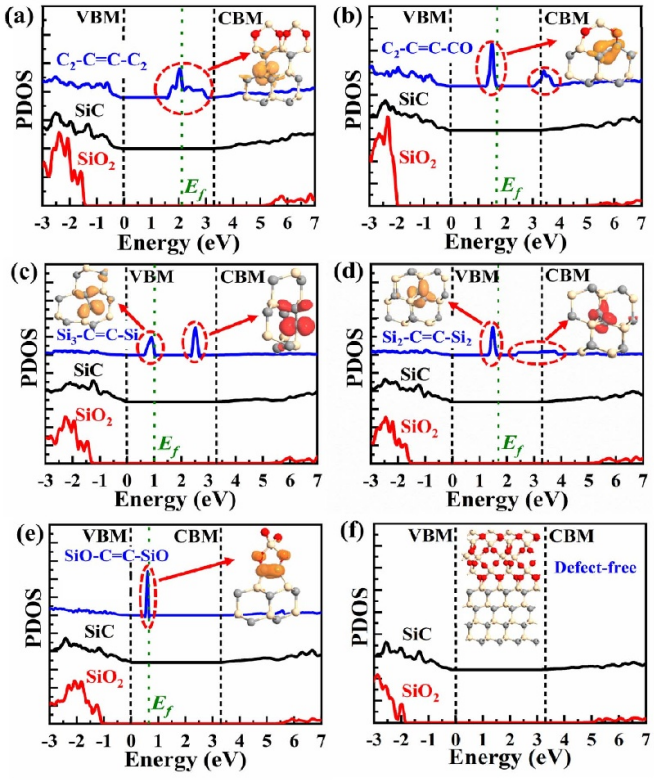

Figure 4. Projected density of states (PDOS) for SiO_2/4H-SiC interface with (a) C_2–C = C–C_2, (b) C_2–C = C–CO, (c) Si_3–C–C–Si, (d) Si_2–C = C–Si_2, (e) SiO–C = C–SiO defect, and (f) defect-free case (for comparison), respectively. Orbitals of defect gap states are inserted. Note that the PDOS of SiC and SiO_2 are taken from the atoms lie far away from the interfacial region. The valence band maximum (VBM) is aligned at 0 eV.

To further illustrate the distribution of electron states for the defect interface, the LDOS was calculated, defined as follows,

$$D(E,r) = \sum_i \sum_k \omega_k |\psi_{i,k}(r)|^2 \delta(E-\varepsilon_{i,k}) = \sum_i \sum_k \omega_k |\psi_{i,k}(r)|^2 \omega(E,\varepsilon_{i,k}), \quad (3)$$

$$\omega(\varepsilon_{i,k}) = \frac{1}{\sqrt{2\pi\sigma^2}} \exp\left(\frac{(E-\varepsilon_{i,k})^2}{2\sigma^2}\right), \quad (4)$$

where i and k represent band indices and wave vectors, respectively, $\psi_{i,k}(r)$ is the wavefunction of the orbital, ω_k and $\omega(E,\varepsilon_{i,k})$ are k-point weights and energy-dependent Gaussian weights, respectively. Figure 5 shows the calculated LDOS of C_2–C = C–C_2, C_2–C = C–CO, Si_3–C = C–Si, Si_2–C = C–Si_2, CO–C = C–CO defect interfaces and we also consider an ideal interface and the stacking-fault type of interfaces with C_2–C = C–C_2, C_2–C = C–CO defects for comparison. Corresponding LDOS illustrates the distribution of the electron states along the (0001) direction of each defect interface. For the 4H-SiC of the interface, a bandgap of ∼3.20 eV is obtained, which is in agreement with the experimental value of 3.26 eV. The bandgap of the SiO_2 region is still underestimated (∼7.5 eV) compared with the experimental value (∼8.9 eV). The carbon–carbon defects also have an impact on the interfacial band lineup, especially the valence band offset. This is largely due to the changes in the symmetry of the interface caused by the defects. The valence band electron states are concentrated layer by layer correspond to each atomic layer of the interface, while the conduction band electron states are not. This is because of the special internal space distribution of the SiC conduction band states [47, 48]. It should be pointed out that gap states are observed in the 4H-SiC bandgap of each interface and corresponding positions in real space are consistent with the locations of corresponding carbon–carbon defects at the interface. The C_2–C = C–C_2 defect states are located at ∼0.5 eV below the CBM (figure 5(a)). The C_2–C = C–CO defect includes two parts, one located at the CBM and the other is located at ∼1.3 eV below the CBM (figure 5(c)). Furthermore, the stacking-fault structures (figures 5(b) and (d)) increase the gap states very close to the CBM. From figures 5(e)–(g), both the interfacial SiO–C = C–SiO and Si_3–C = C–Si defects introduce the gap states located at ∼1.0 eV above the VBM, while the latter defect also introduces other gap states located at ∼0.5 eV below the CBM. The gap states induced by the Si_2–C = C–Si_2 defect are very similar to the stacking-fault interface with the C_2–C = C–C_2 defect.

3.3. Defect CTLs

To further understand the intrinsic properties of the carbon–carbon defects in the improved thermal oxidation process, the formation energies of charged defects (E_{form}) [49] at the interfaces were calculated under C-rich and O-poor conditions (figure 6). For the charged defects, we applied a Finite-Size Supercell Correction scheme based on the classical electrostatic potential [49, 50] to overcome the divergence of formation energy with the size of the vacuum region. We obtained the electrostatic potential along the c-direction of the defect interface and perfect model based on the self-consistently from the electronic-structure calculation [49–51]. Additional structure and calculations can be seen in figures S1 and S2 (available online at stacks.iop.org/JPD/55/025109/mmedia). From figure 6(a), each defect has stable charge states with the variation of Fermi level. Among these defects, the interfacial C_2–C = C–CO defect has the lowest E_{form}, while the interfacial Si_2–C = C–Si_2 defect has the highest E_{form}, indicating the C_2–C = C–CO defect at the SiO_2/4H-SiC interface is more stable under O-poor and C-rich conditions. Interestingly, the stacking-fault type with defect (type-IV) shows more stable than the normal type. The formation energy of interfacial C_2–C = C–C_2 defect is comparable with the [(C_2)Si] defect [14]. For C = C defects, the negatively-charged and positively-charged states are more stable than the corresponding neutral state under n-type and p-type growth conditions, respectively. The CTLs of each carbon–carbon defect are summarized in figure 6(b). The 0/− CTLs of defects mainly locate within ∼0.8 eV below CBM, acting as acceptors. However, +/0 CTLs are different. Interestingly, the 0/−1 CTLs of type-I

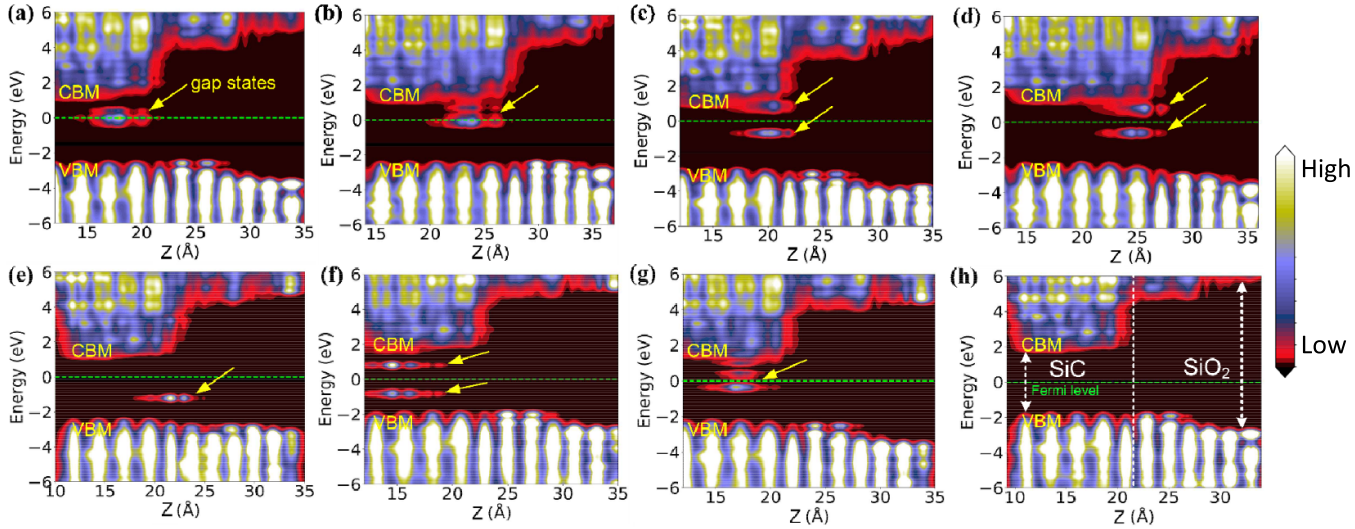

Figure 5. Local density of states (LDOS) for SiO_2/4H-SiC interface with (a) C_2–C = C–C_2, (b) stacking-fault with C_2–C = C–C_2, (c) C_2–C = C–CO, (d) stacking-fault with C_2–C = C–CO, (e) SiO–C = C–SiO, (f) Si_3–C = C–Si, (g) Si_2–C = C–Si_2 defect and (h) defect-free case (for comparison). Note that the electron states are projected along the *z*-direction of the interface slab model. The magnitude of LDOS is indicated by the color code shown in the bottom. The green line represents the Fermi level set to 0 eV.

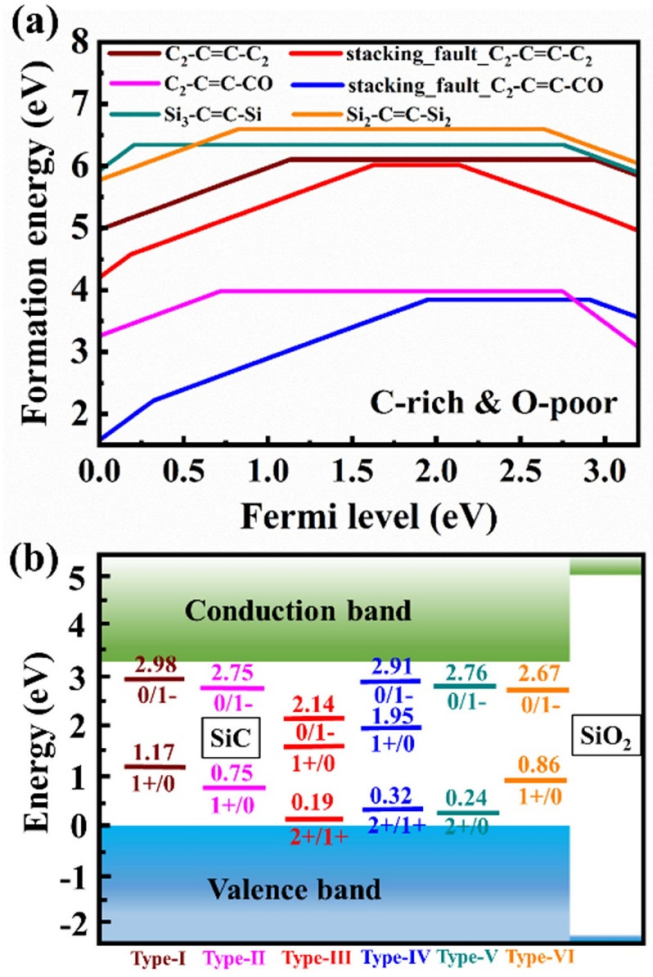

Figure 6. (a) Formation energies as a function of Fermi level and (b) diagram of CTLs for carbon–carbon defects at SiO_2/4H-SiC interfaces. Note that all the results were calculated by HSE06 hybrid functional. The type-I to type-VI represents the C_2–C = C–C_2, stacking-fault with C_2–C = C–C_2, C_2–C = C–CO, stacking-fault with C_2–C = C–CO, Si_3–C = C–Si and Si_2–C = C–Si_2 defect, respectively.

and type-IV defects only locate within ∼0.30 eV below CBM and the negatively-charged states are more stable in n-type SiC. The results are very close to the di-carbon anti-site in bulk 4H-SiC, where the 0/−1 CTL of (C_2)Si(h) locates at 0.10 eV below CBM [14]. This is also another evidence to prove that C = C defects at the interface could be one of the possible factors for the poor performance of n-channel SiC-MOSFETs.

4. Conclusion

The atomic and electronic structures of five types of carbon–carbon defects at the SiO_2/4H-SiC (0001) interface are investigated by first-principles calculation in detail. For the thermal oxidation of 4H-SiC, the variation of the interfacial chemical potentials indicates the formation of carbon-related defects. Furthermore, the interfacial carbon–carbon defects are easy to form under C-rich and O-rich oxidation conditions, while they are hard to form under oxygen-poor conditions. From the calculated electronic structures, the carbon–carbon defects all induce gap states, which are mainly located near the Fermi level and caused by the carbon-p anti-bonding orbitals. The interfacial carbon–carbon defects on SiC side tend to induce the gap states near the CBM, while the gap states caused by the defects in the SiO_2 layer are mainly located near the VBM. Furthermore, the stacking-fault of SiC will intensify the gap states below the CBM. The calculated CTLs further show the 0/− CTLs of our introduced carbon–carbon defects act as acceptors close to the CBM. All the theoretical results prove that the interfacial carbon–carbon defects could be one of the most important factors responsible for the poor performance of n-channel SiC-MOSFETs. It is also suggested that developing more effective oxidation methods to avoid carbon–carbon defects is favorable for improving the performance of SiC-MOSFETs.

Data availability statement

All data that support the findings of this study are included within the article (and any supplementary files).

Acknowledgments

This work was supported by the Wuhan University Junior Faculty Research (No. 2042019KF0003), the National Natural Science Foundation of China (Nos. 51727901, 62174122 and U1501241), the National Key R&D Program of China (No. 2017YFB1103904), and the Hubei Provincial Natural Science Foundation of China (No. 2020CFA032). The numerical calculations in this article have been done on the supercomputing system in the Supercomputing Center of Wuhan University.

ORCID iDs

Zhen Wang https://orcid.org/0000-0003-2334-1804
Zhaofu Zhang https://orcid.org/0000-0002-1406-1256
John Robertson https://orcid.org/0000-0001-6558-528X
Yuzheng Guo https://orcid.org/0000-0001-9224-3816

References

[1] Tsao J Y *et al* 2018 *Adv. Electron. Mater.* **4** 1600501
[2] Bindra A 2018 *IEEE Power Electron. Mag.* **5** 22
[3] Kimoto T and Cooper J A 2014 *Fundamentals of Silicon Carbide Technology* (Singapore: John Wiley and Sons) (https://doi.org/10.1002/9781118313534)
[4] Kimoto T 2015 *Japan. J. Appl. Phys.* **54** 40101
[5] Pensl G *et al* 2008 *Phys. Status Solidi* b **245** 1378
[6] Rozen J, Ahyi A C, Zhu X, Williams J R and Feldman L C 2011 *IEEE Trans. Electron Devices* **58** 3808
[7] Yoshioka H, Senzaki J, Shimozato A, Tanaka Y and Okumura H 2014 *Appl. Phys. Lett.* **104** 83516
[8] Kobayashi T, Nakazawa S, Okuda T, Suda J and Kimoto T 2016 *Appl. Phys. Lett.* **108** 152101
[9] Afanas Ev V V, Stesmans F, Ciobanu G, Pensl K, Cheong Y and Dimitrijev S 2003 *Appl. Phys. Lett.* **82** 568
[10] Noborio M, Suda J, Beljakowa S, Krieger M and Kimoto T 2009 *Phys. Status Solidi* a **206** 2374
[11] Zhu X, Lee H D, Feng T, Ahyi A C, Mastrogiovanni D, Wan A, Garfunkel E, Williams J R, Gustafsson T and Feldman L C 2010 *Appl. Phys. Lett.* **97** 71908
[12] Li X *et al* 2018 *Appl. Phys. Lett.* **113** 131601
[13] Zhang F, Yang C, Su Y and Wang D 2020 *Appl. Surf. Sci.* **20** 145889
[14] Kobayashi T, Harada K, Kumagai Y, Oba F and Matsushita Y 2019 *J. Appl. Phys.* **125** 125701
[15] Devynck F, Alkauskas A, Broqvist P and Pasquarello A 2011 *Phys. Rev.* B **83** 195319
[16] Devynck F, Alkauskas A, Broqvist P and Pasquarello A 2011 *Phys. Rev.* B **84** 235320
[17] Anders M A, Lenahan P M and Lelis A J 2016 *Appl. Phys. Lett.* **109** 142106
[18] Kaneko T, Tajima N, Yamasaki T, Nara J, Schimizu T, Kato K and Ohno T 2018 *Appl. Phys. Express* **11** 11302
[19] Cottom J, Gruber G, Pobegen G, Aichinger T and Shluger A L 2018 *J. Appl. Phys.* **124** 45302
[20] Kobayashia T and Matsushita Y 2019 *J. Appl. Phys.* **126** 145302
[21] Umeda T, Kobayashi T, Sometani M, Yano H, Matsushita Y and Harada S 2020 *Appl. Phys. Lett.* **116** 71604
[22] Wang S, Dhar S, Wang S R, Ahyi A C and Pantelides S T 2007 *Phys. Rev. Lett.* **98** 26101
[23] Deak P, Knaup J M, Hornos T, Thill C, Gali A and Frauenheim T 2007 *J. Phys. D: Appl. Phys.* **40** 6242
[24] Okamoto D, Yano H, Hatayama T and Fuyuki T 2010 *Appl. Phys. Lett.* **96** 203508
[25] Liu G, Ahyi A C, Xu Y, Isaacs-Smith T, Sharma Y K, Williams J R, Feldman L C and Dhar S 2013 *IEEE Electron Device Lett.* **34** 181
[26] Matsushita Y and Oshiyama A 2017 *Nano Lett.* **17** 6458
[27] Kobayashi T, Okuda T, Tachiki K, Ito K, Matsushita Y and Kimoto T 2020 *Appl. Phys. Express* **13** 91003
[28] Tachiki K, Kaneko M, Kobayashi T and Kimoto T 2020 *Appl. Phys. Express* **13** 121002
[29] Iwase S, Kirkham C J and Ono T 2017 *Phys. Rev.* B **95** 41302
[30] Liu G, Tuttle B R and Dhar S 2015 *Appl. Phys. Rev.* **2** 21307
[31] Potbhare S, Goldsman N, Pennington G, Lelis A and McGarrity J M 2006 *J. Appl. Phys.* **100** 44511
[32] Lichtenwalner D J, Cheng L, Dhar S, Agarwal A and Palmour J W 2014 *Appl. Phys. Lett.* **105** 182107
[33] Blöchl P E 1994 *Phys. Rev.* B **50** 17953
[34] Kresse G and Joubert D 1999 *Phys. Rev.* B **59** 1758
[35] Monkhorst H J and Pack J D 1976 *Phys. Rev.* B **13** 5188
[36] Perdew J P, Burke K and Ernzerhof M 1996 *Phys. Rev. Lett.* **77** 3865

[37] Heyd J, Scuseria G E and Ernzerhof M 2006 *J. Chem. Phys.* **124** 219906
[38] Zhang Z, Guo Y and Robertson J 2019 *Appl. Phys. Lett.* **114** 161601
[39] Wang Z, Zhang Z, Shao C, Robertson J, Liu S and Guo Y 2020 *Appl. Surf. Sci.* **527** 146843
[40] Wang Z, Zhang Z, Shao C, Robertson J, Liu S and Guo Y 2021 *IEEE Trans. Electron Devices* **68** 288
[41] Fukuda K, Kato M, Kojima K and Senzaki J 2004 *Appl. Phys. Lett.* **84** 2088
[42] Zhang Z, Wang Z, Guo Y and Robertson J 2021 *Appl. Phys. Lett.* **118** 031601
[43] Son N T, Trinh X T, Løvlie L S, Svensson B G, Kawahara K, Suda J, Kimoto T, Umeda T, Isoya J and Makino T 2012 *Phys. Rev. Lett.* **109** 187603
[44] Umeda T, Kim G-W, Okuda T, Sometani M, Kimoto T and Harada S 2018 *Appl. Phys. Lett.* **113** 61605
[45] Tromp R M, Medhekar N V, Shenoy V B and Hannon J B 2009 *Phys. Rev. Lett.* **103** 256101
[46] Tsuchida H, Ito M, Kamata I and Nagano M 2009 *Phys. Status Solidi* b **246** 1553
[47] Furuya S, Oshiyama A and Matsushita Y 2012 *Phys. Rev. Lett.* **108** 246404
[48] Oshiyama A and Matsushita Y 2014 *Phys. Rev. Lett.* **112** 136403
[49] van de Walle C G and Neugebauer J 2004 *J. Appl. Phys.* **95** 3851
[50] Pasquarello A and Komsa H 2013 *Phys. Rev. Lett.* **110** 95505
[51] Lyons J L, Janotti A and van de Walle C G 2012 *Phys. Rev. Lett.* **108** 156403